CREATINE KINASE-DEPENDENT ENERGY TRANSPORT IN SEA URCHIN SPERMATOZOA

Flagellar Wave Attenuation and Theoretical Analysis of High Energy Phosphate Diffusion

ROBERT M. TOMBES,* CHARLES J. BROKAW,‡ and BENNETT M. SHAPIRO*
*Department of Biochemistry, University of Washington, Seattle, Washington 98195; and ‡Division of Biology, California Institute of Technology, Pasadena, California 91125

ABSTRACT The significance of a phosphocreatine (PCr) shuttle in the energy transport of motile spermatozoa (Tombes, R. M., and B. M. Shapiro, 1985, *Cell*, 41:325–334) has been tested by a quantitative analysis of motility. Computer-assisted analysis of stroboscopic photomicrographs of live sea urchin spermatozoa whose creatine kinase has been specifically inhibited by fluorodinitrobenzene reveals that motility is impaired due to a progressive damping of bending waves as they propagate along the flagellum. This lesion, which has been defined as attenuation and can be quantified, is repaired when these spermatozoa are demembranated and reactivated to swim with ATP. The implication that attenuation is due to the inhibition of energy transport via a PCr shuttle resulting in the decrease of ATP and accumulation of inhibitory levels of ADP distally has been supported by calculating sperm PCr and ATP levels resulting from diffusion along the flagellum. The specific alterations of motility seen with creatine kinase inhibition and their reversal with ATP are as expected from the model and provide strong support for the PCr shuttle in high energy phosphate transport.

INTRODUCTION

An active microtubule sliding mechanism, distributed along the entire length of the axoneme, is responsible for the propagation of constant amplitude bending waves along sea urchin sperm flagella (reviewed in Gibbons, 1981). This microtubule sliding consumes ATP; mechanochemical coupling is effected by the dynein ATPase, located along the axoneme (reviewed in Warner and Mitchell, 1980). Sufficient ATP must be provided at all dynein sites: in demembranated sea urchin sperm flagella, axonemal bending begins at a threshold (5 μM) ATP concentration and flagellar beat frequency increases with increasing ATP concentration (Brokaw, 1967, 1975; Penningroth et al., 1982; Gibbons and Gibbons, 1972). Biochemical and geometrical aspects of the sea urchin sperm set important constraints upon any mechanism for providing ATP to dynein sites along the flagellum.

Energy generation in sea urchin sperm is almost completely done by fatty acid oxidation (Rothschild and Cleland, 1952; Mita and Yasumasu, 1983; Hansbrough et al., 1980) in a single mitochondrion located at the base of the sperm head (Baccetti and Afzelius, 1976). Motile sperm respire maximally (i.e., oxygen consumption does not increase with addition of uncoupling agents; Christen et al., 1983*a*) and dynein ATPase accounts for virtually all of the ATP that is used (Christen et al., 1982, 1983*a*). Since active microtubule sliding occurs all along the axoneme, the spermatozoa must be capable of providing sufficient ATP at the distal end of the flagellum, some 40 μm from the mitochondrion, while maintaining a sufficiently high ADP concentration at the mitochondrion to act as the substrate for rapid, tightly coupled respiration.

The earliest calculations of ATP diffusion along a sea urchin sperm flagellum (Brokaw, 1966) concluded that the supply of ATP by diffusion would be adequate if an ATP concentration of at least 4 mM was maintained at the base of the flagellum. However, this calculation used a diffusion coefficient for ATP in aqueous solutions, while other measurements have suggested that the actual value for ATP diffusion in muscle fibers is only about one-half the value for diffusion in aqueous solutions (Bowen and Martin, 1963). A reduced diffusion coefficient resulting from the space occupied by the high concentration of muscle proteins is also likely to be appropriate for diffusion in a flagellum, where much of the cross-section is occupied by microtubules and other proteins. Additionally, new work (Brokaw and Gibbons, 1975; Christen et al., 1982, 1983*a*) indicates that the rate of ATP utilization by sea urchin flagella is 50–100% greater than the value used in the 1966 calculation. These considerations suggest that ATP diffusion alone may not be sufficient for adequately supplying

energy to these flagella, unless an unrealistically high ATP concentration at the base of the flagellum is assumed.

Recent evidence implicates phosphocreatine (PCr) as the major vehicle for energy transport from sperm mitochondrion to tail (Tombes and Shapiro, 1985). Sea urchin sperm have high PCr levels (Christen et al., 1983*b*) and separate isozymes of creatine kinase (CrK) in the head and tail regions (Tombes and Shapiro, 1985). Fluorodinitrobenzene (FDNB), under conditions that appear to be specific for the inhibition of CrK, inhibits sperm motility and respiration, a finding compatible with the coupling of mitochondrial and axonemal functions via a PCr shuttle (Tombes and Shapiro, 1985). Such metabolite channeling, implied by a PCr shuttling mechanism, might be of general relevance to cellular regulation in systems other than the spermatozoa. However, arguments for its existence are dependent upon the specificity of the FDNB reaction with intact spermatozoa. The previous study (Tombes and Shapiro, 1985) indicated that the principal targets for FDNB were the CrK isozymes, and that motility and respiration were both affected as anticipated. The nature of the motility alteration upon CrK inhibition provides an important test of the hypothesis. If a PCr shuttle were operative in spermatozoa, then inhibition of the shuttling mechanism would lead to a specific motility lesion; the distal portion of the sperm tail should be more affected, since ATP diffusion would be inadequate for energy distribution to the flagellar tip. Moreover, subsequent provision of ATP to distal flagellar sites should lead to normal motion.

The previous experiments (Tombes and Shapiro, 1985) did not examine motility with sufficient resolution to determine the specificity of the alteration. In this paper we provide a quantitative analysis of the reduction in flagellar bending in the distal portion of the flagellum as CrK is inhibited and show that demembranated, CrK-inhibited spermatozoa have normal axonemal bending parameters upon reactivation with ATP. An analysis of energy diffusion from sperm mitochondrion to tail that determines the effects of CrK inhibition on ATP use along the flagellum strongly supports the involvement of a PCr shuttle.

METHODS

Analysis of Sperm Motility and CrK Activity

Spermatozoa from the sea urchin, *Strongylocentrotus purpuratus*, were obtained by intracoelomic injection of 0.5 M KCl. All observations were carried out within 12 h of spawning and were performed at 18°C unless otherwise indicated. Spermatozoa were treated with FDNB as previously described (Tombes and Shapiro, 1985) by diluting dry spermatozoa approximately 10-fold to 4×10^9 cells/ml with the appropriate concentration of FDNB. Observations were made between 2 and 10 h after initiation of the reaction, since CrK activity is inhibited maximally within 2 h (Tombes and Shapiro, 1985). High potassium artificial seawater containing 100 mM KCl and 30 mM HEPES buffer, pH 8.0 (Christen et al., 1983*a*) was used as the medium for incubating sperm with FDNB, although Millipore-filtered seawater (MFSW), buffered similarly, worked as well at high sperm concentrations (10%) to preserve sperm viability during incubations with FDNB. The effect of FDNB on sperm motility was similar regardless of whether 100 mM KCl was present in the medium or not. Iodosobenzoic acid (Sigma Chemical Co., St. Louis, MO) was prepared identically to FDNB.

To observe motility, sperm incubated with or without FDNB were diluted 10,000-fold to 4×10^5 cells/ml in MFSW containing 0.5% polyvinylpyrollidone (PVP). The first 25 spermatozoa encountered in observations at the top surface of an open drop were photographed using dark-field stroboscopic illumination by a photographer who was not informed about the FDNB treatment history of each sample. Photographic images were digitized and processed by microcomputer programs (Brokaw, 1984*b*) to obtain flagellar wave parameters characteristic of each sample. Photography of spermatozoa in each sample was usually completed within 5 min.

Demembranated spermatozoa were prepared by diluting the 4×10^9 sperm/ml suspension 20-fold into 0.04% Triton X-100, 150 mM KCl, 10 mM Tris, pH 8.2, 1 mM dithiothreitol (DTT), 2 mM $MgSO_4$, 1 mM EGTA, 0.2 mM ATP, and 0.01 mM cAMP. After 30 s, this was diluted another 10-fold into 150 mM KCl, 10 mM Tris, pH 8.2, 1 mM DTT, 2.2 mM $CaCl_2$, and 0.01% Triton X-100. This suspension (0.01 ml) was diluted into reactivation solution (0.5 ml) containing 250 mM K^+ acetate, 10 mM Tris, pH 8.2, 1 mM DTT, 0.5% polyethyleneglycol, 2 mM EDTA, 0.2 mM EGTA, 4.63 mM $MgSO_4$, and 0.53 mM ATP. A drop of this suspension was observed, photographed, and processed as above.

CrK activities were determined by diluting a 4×10^9 sperm/ml suspension 20-fold into 0.04% Triton X-100, 10 mM Tris, pH 8.0, 5 mM $MgCl_2$, 150 mM KCl, 1 mM EGTA, and 1 mM DTT and assayed spectrophotometrically at 25°C as previously described (Tombes and Shapiro, 1985).

Calculation of High Energy Phosphate (~P) Diffusion along the Flagellum

Each molecular species diffusing along the flagellum is governed by a diffusion equation

$$\partial C(s, t)/\partial t = D \cdot \partial^2 C(s, t)/\partial s^2 + Q(s, t), \qquad (1)$$

where C represents the concentration of the diffusing species, D is the relevant diffusion coefficient, s is the coordinate measuring position along the length of the flagellum, and Q is the rate of production of the species by chemical reactions. We need to consider three reactions, specified by Q_1, Q_2, and Q_3.

Q_1 is the dynein ATPase rate. Since the use of ATP by flagella is tightly coupled to motility, we will assume that the relationship between the ATPase rate and the ATP concentration is similar to the relationship between flagellar beat frequency and ATP concentration.

$$Q_1 = Q_{1F} / (1 + K1(1 + [ADP] / K_I/[ATP]), \qquad (2)$$

where $K1$ is the ATP concentration for half-maximal beat frequency, and K_I is the constant for competitive inhibition of the beat frequency by ADP. For the maximum rate, Q_{1F}, we use a value of 0.0034 M/s, based on measurements of respiration in *S. purpuratus* spermatozoa (Brokaw and Gibbons, 1975; Brokaw, 1986; Tombes, R. M., unpublished data). For $K1$ we use values obtained from measurements on demembranated spermatozoa from two other sea urchin species, in reactivation solutions containing acetate as the major anion (Brokaw, 1984*a*; Gibbons et al., 1985); in both cases the value obtained was 0.11 mM. For K_I, we use a value of 0.22 mM, based on measurements indicating that the value of K_I for demembranated sea urchin sperm flagella was twice the value of $K1$ (Okuno and Brokaw, 1979). The reverse reaction for the ATPase is neglected.

Q_2 is the rate for the adenylate kinase reaction (Noda, 1973):

$$\text{ATP} + \text{AMP} \longrightarrow 2\ \text{ADP}.$$

For this reaction, both forward and reverse rates are considered:

$$Q_2 = \left(Q_{2F}\frac{[ATP]\,[AMP]}{K_N \cdot K_M} - Q_{2R}\frac{[ADP]\,[ADP]}{K_A \cdot K_A}\right) \Bigg/ \left(1 + \frac{[ATP]\,[AMP]}{K_N \cdot K_M} + \frac{[ADP]\,[ADP]}{K_A \cdot K_A} + \frac{[ATP]}{K_N} + \frac{[AMP]}{K_M} + \frac{2[ADP]}{K_A}\right). \quad (3)$$

Values used for the parameters in this expression are given in Table I.

Q_3 is the rate for the CrK reaction:

$$ATP + Cr \longrightarrow ADP + PCr.$$

For this reaction also, both forward and reverse rates are considered:

$$Q_3 = \left(Q_{3F}\frac{[ATP]\,[Cr]}{K_T \cdot K_C} - Q_{3R}\frac{[ADP]\,[PCr]}{K_D \cdot K_P}\right) \Bigg/ \left(1 + \frac{[ATP]\,[Cr]}{K_T \cdot K_C} + \frac{[ADP]\,[PC]}{K_D \cdot K_P} + \frac{[ATP]}{K_T} + \frac{[ADP]}{K_D} + \frac{[Cr]}{K_C} + \frac{[PCr]}{K_P}\right) \quad (4)$$

and values used for the parameters in this expression are given in Table I.

For each species, Q is a sum of the relevant rates: For ATP, $Q = -Q_1 - Q_2 - Q_3$; for ADP, $Q = Q_1 + 2Q_2 + Q_3$; for AMP, $Q = -Q_2$; for PCr, $Q = Q_3$; and Cr, $Q = -Q_3$. This can be simplified, since if we assume that the diffusion coefficients for ATP, ADP, and AMP are equal and PCr and Cr are equal, there will be no gradient of total adenine nucleotide or total Cr concentration along the flagellum. Thus, AMP can be obtained from (total adenine nucleotide − ATP − ADP) and Cr can be obtained from total (Cr + PCr) − PCr, without integrating the differential equation for either compound. This is probably a good approximation for dealing with the adenine nucleotides, which have relatively similar molecular weights, but is less valid for Cr and PCr, leading to an overestimation of the magnitude of the Cr gradient along the flagellum.

To solve the system of partial differential equations, each having the form of Eq. 1, for ATP, ADP, and PCr, we used the approach introduced by Lin (1972), and integrated the three equations forward with time until a steady equilibrium solution was obtained. Concentrations at the basal end of the flagellum were held constant, and no fluxes were allowed past the distal end of the flagellum. Although Lin used an efficient Crank–Nicholson method for integrating the equations, we found that it was feasible to use a simple explicit method with long computing times and sufficiently small time steps to ensure stability. For each species, Eq. 1 was converted to:

$$C(s, t + \Delta t) = C(s, t) + D[(C(s - \Delta s, t) - 2C(s, t) + C(s + \Delta s, t)) / \Delta s^2] + Q(s, t) \cdot \Delta t. \quad (5)$$

The length interval, Δs, was 1 μm in all the results shown, and the time interval, Δt, was normally 1 ms. This method was validated by using it to solve the simple zero-order ATP diffusion problem, and by performing computations with smaller time and length intervals.

RESULTS

Definition of Bending Wave Attenuation

For each spermatozoon that was analyzed, four to six photographic images of the sperm flagellum, covering

TABLE I
PARAMETERS USED FOR COMPUTATIONS OF ~P TRANSPORT IN FLAGELLA

Parameter	Value	Reference
Flagellar length	40 μm	Brokaw and Gibbons, 1975, and these data
Diffusion coefficient for ATP, ADP, and AMP	150 $\mu m^2/s$	Kushmerick and Podolsky, 1969
Diffusion coefficient for Cr and PCr	260 $\mu m^2/s$	Same as above
Total Cr and PCr	20 mM	Not measured
PCr at base of flagellum	16 mM	Average from Christen et al., 1983*b*; Nevo and Rikmenspoel, 1970; Mita and Yasumasu, 1983 using sperm volumes and protein values listed below
Total adenine nucleotide	6 mM	
Mean ATPase rate	3.4 mM/s	See text
$K1$ (K_m of ATPase from ATP, from ATP concentration for half-maximal beat frequency of demembranated flagella)	0.11 mM	Brokaw, 1984*a*; Gibbons et al., 1985
K_I (for inhibition of flagellar beat frequency by ADP)	0.22 mM	Okuno and Brokaw, 1979
Q_{2R} (adenylate kinase reverse rate)	3.4 mM/s	Brokaw and Gibbons, 1973
Q_{2R}/Q_{2F} (ratio of reverse to forward adenylate kinase)	1.0	Noda, 1973
K_A, K_N, K_M (myokinase K_m values for ATP, ADP, and AMP, respectively)	0.3 mM	Noda, 1973
Q_{3R} (CrK reverse rate)	12.5 mM/s	To fit results; see text
Q_{3R}/Q_{3F} at pH 7.5 (ratio of reverse to forward CrK rates)	4.7	Tombes, R.M., and B.M. Shapiro, manuscript in preparation
K_m's for flagellar CrK		
K_C (Cr)	50 mM	Tombes, R.M., and B.M. Shapiro, manuscript in preparation
K_T (ATP)	0.43 mM	Same as above
K_P (PCr)	6 mM	Same as above
K_D (ADP)	0.12 mM	Same as above
Protein content of whole sperm	6×10^8 sperm/mg	Tombes and Shapiro, 1985, and unpublished data
Protein content of isolated flagella	2.5×10^9 whole flagella/mg	
Cytoplasmic volume	7×10^{-15} liters/sperm	Schackmann et al., 1984
Intracellular pH of motile sperm	7.5	Christen et al., 1982

approximately one beat cycle, were digitized and entered into a microcomputer. The data were differentiated and filtered to give graphs of the curvature of the flagellum as a function of length (Brokaw, 1984*b*). The graphs were then used to obtain a set of parameters describing the propagation of bending waves by this flagellum, by using a "constant curvature" model for the flagellar bending waves (Brokaw, 1983, 1984*b*). In this model, the bends are represented by circular arcs, and the interbend regions are regions in which the curvature changes linearly from the value characteristic of one bend to the value characteristic of the next bend. Bends move at constant velocity along the flagellum. As suggested previously (Brokaw, 1984*b*), an improved fit of the model to the data was often obtained by allowing the characteristic curvature of each bend to change linearly as the bend moved along the flagellum. This modification turned out to be particularly useful for dealing with the bending waves considered in this paper, in which decreased bending in the distal region of the flagellum was observed after treatment of the spermatozoa with FDNB.

To describe this decreased bending in the distal region of the flagellum, we define a new parameter, which we will call the attenuation of the bending waves. The attenuation measures the fractional reduction in curvature of the flagellar bends at the distal end of the flagella, compared with the curvature at the basal end. The attenuation is calculated from the following formula:

$$\text{Attenuation} = 2(R\text{curvslope} - P\text{curvslope}) \,/\, (R\text{curvslope} - P\text{curvslope} - 2(R\text{curv} - P\text{curv})/S). \quad (6)$$

In this formula, S is the length of the flagellum. *R*curv and *P*curv are values for the characteristic curvatures of reverse and principal bends, respectively, measured at the midpoint of the flagellar length. Principal and reverse bends are defined so that the asymmetry of the flagellum is positive, which usually means that the magnitude of *P*curv is greater than the magnitude of *R*curv. By convention, the sign of *P*curv is negative and that of *R*curv is positive (cf. Fig. 2). *R*curvslope and *P*curvslope are, respectively, the linear rates of change of the curvature of reverse and principal bends with length.

In a bending wave that propagates along the flagellum with constant curvature, the values of *R*curvslope, *P*curvslope, and attenuation are all zero. A value of attenuation of 1.0 corresponds to a bending wave in which the curvatures of the bends decrease to zero at the distal end of the flagellum. For a symmetrical bending wave, this means that $P\text{curvslope} = -2P\text{curv}/S$ and $R\text{curvslope} = -2R\text{curv}/S$.

Effects of FDNB Treatment on Bending Wave Attenuation

Fig. 1 *a* shows a photograph of a typical spermatozoon from a control sample not treated with FDNB. Analysis of this spermatozoon, shown in Fig. 2 *A*, yields an attenuation value of 0.34. This spermatozoon was from a sample of 20 spermatozoa from a single drop (see Methods) for which a mean value of 0.41 ± 0.15 (standard deviation) was obtained for the attenuation. For eight such control samples that were analyzed, the mean attenuation values ranged from 0.28 to 0.44, with a mean of 0.35 ± 0.07; the standard deviations for these samples ranged from 0.07 to 0.17.

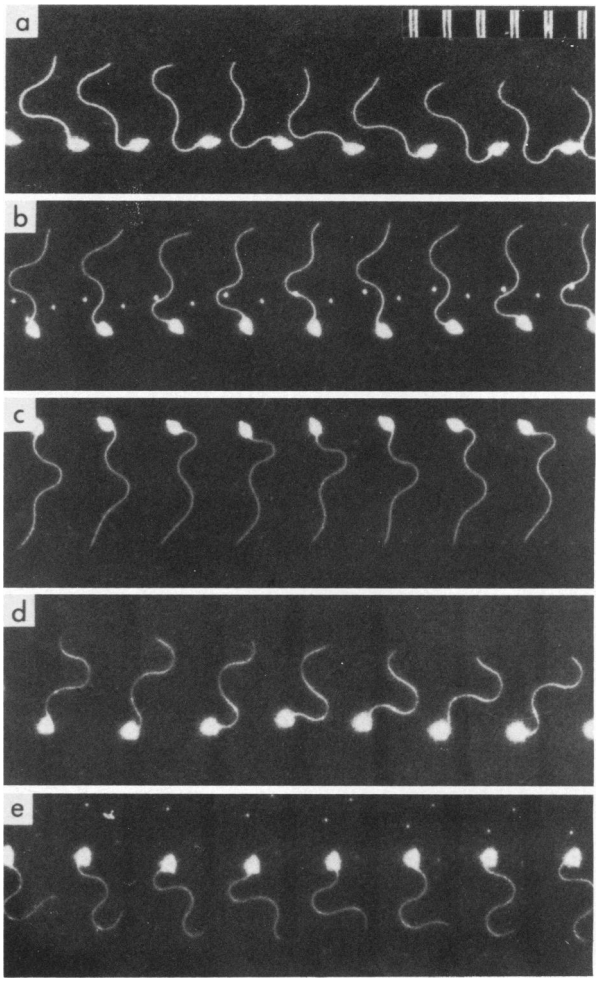

FIGURE 1 Examples of photographs used for analysis of flagellar bending waves. Taken on moving film with strobe flashes at 120 Hz. The scale marker represents 10-μm intervals. (*a*) Live spermatozoa, no FDNB treatment; attenuation value is 0.34. (*b*) Live spermatozoa, treated with 15 μM FDNB; attenuation value is 0.68. (*c*) Live spermatozoa, treated with 15 μM FDNB; attenuation value is 0.95. (*d*) Demembranated spermatozoa, no FDNB treatment; attenuation value is 0.2. (*e*) Demembranated spermatozoa after treatment with 15 μM FDNB; attenuation value is 0.3.

Fig. 1 *b* shows a photograph of a typical spermatozoon from a sample treated with 15 μM FDNB. Analysis of this spermatozoon, shown in Fig. 2 *B*, yields an attenuation value of 0.68. This spermatozoon was from a sample of 20 spermatozoa for which a mean value of 0.68 ± 0.10 was obtained for the attenuation. The values of attenuation in this sample ranged from 0.54 to 0.95. The spermatozoon

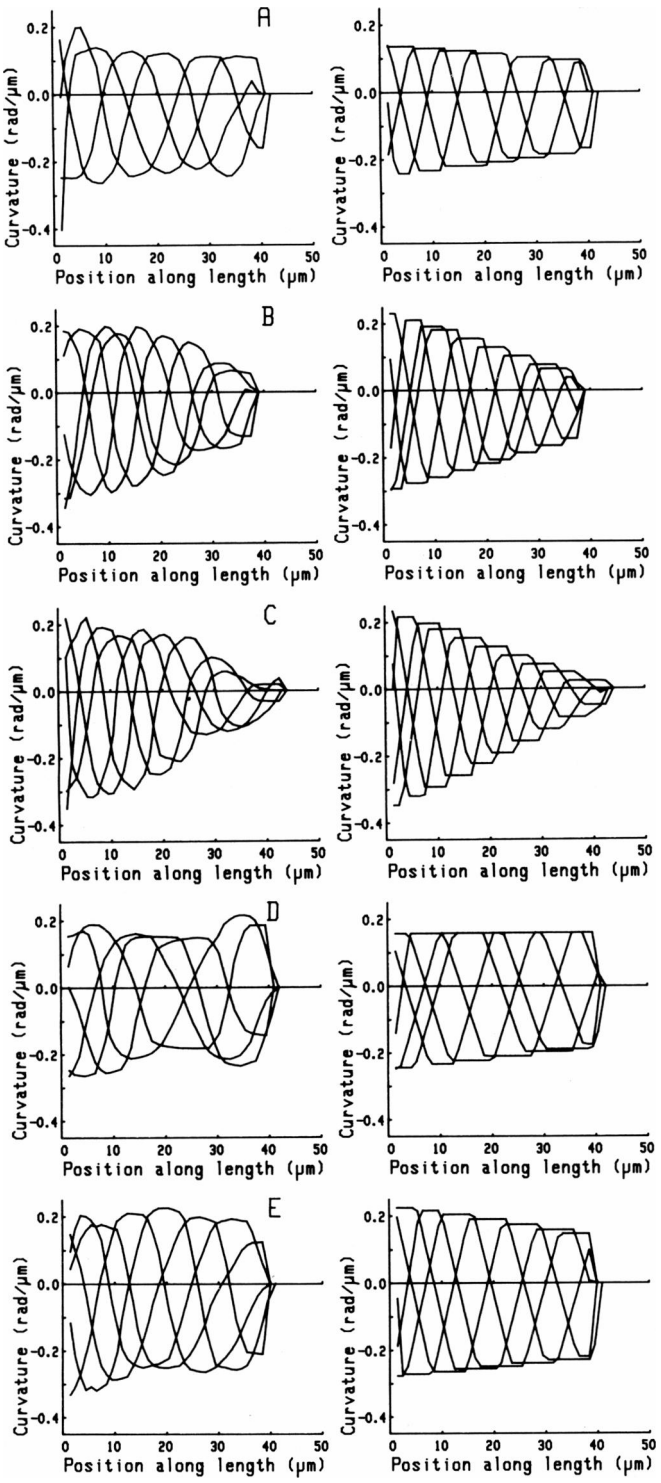

FIGURE 2 Examples of data obtained from photographs of flagellar bending waves, after digitization, filtering, and differentiation to obtain plots of curvature vs. position along the length of the flagellum. (*Left*) Data plots; (*right*) results obtained by fitting the constant curvature model to the data curves by a Simplex method that minimizes the root-mean-square differences between the data curves and the model curves (Brokaw, 1984*b*). *A–E* are obtained from the corresponding examples in Fig. 1.

with the highest value of attenuation in this sample is shown in Fig. 1 *c*. It was always possible to search through the FDNB-treated samples and find many examples of spermatozoa with extremely attenuated bending waves, similar to or more extremely attenuated than the example shown in Fig. 1 *c*, but these represent a minority of the spermatozoa in the samples. They increase in number after the sample has been standing on the microscope slide for 5 or 10 min. Respiration, and thus energy provision, decreases after 10–15 min, as does viability of sperm (unpublished observations). However, attempts to increase the degree of attenuation artificially by examining FDNB-treated sperm in viscous media containing 0.2% methylcellulose were unsuccessful (data not shown).

Selected examples of demembranated, reactivated, sea urchin spermatozoa are shown in Fig. 1, *d* and *e*. Fig. 1 *d* shows an example from a control sample; it has an attenuation of 0.2 that is typical of the value of 0.26 ± 0.14 that was obtained with this sample. Fig. 1 *e* shows an example from a sample that had been treated with 15 μM FDNB before demembranation; it has an attenuation of 0.3 that is typical of the value of 0.34 ± 0.10 that was obtained with this sample. In each of these samples, the maximum value of attenuation was 0.50.

Fig. 3 *A* summarizes results obtained from attenuation measurements on 47 samples of live spermatozoa and 19 samples of demembranated spermatozoa, after treatment with FDNB concentrations ranging from 0 to 50 μM. With the live spermatozoa, no change in attenuation was seen up to a threshold concentration of ~2 μM FDNB. Between 2 and 10 μM FDNB there was a clear increase in attenuation, which appeared to saturate at a level between 0.6 and 0.7, with little or no further increase above 10 μM. The half-maximal point for this attenuation change appeared to be at ~6 μM FDNB. Similar results (now shown) were obtained from less extensive experiments with another CrK inhibitor, iodosobenzoic acid; less information is available about the specificity of CrK inhibition by this reagent.

In contrast to the results observed with live spermatozoa, there was only a very gradual increase in attenuation of reactivated, demembranated spermatozoa as the concentration used for pre-treatment with FDNB was increased from 0 to 50 μM (Fig. 3 *A*). No change specific to the 2–10 μM concentration region is evident.

Effects of FDNB Treatment on Other Bending Wave Parameters

Fig. 3 *B* shows effects of FDNB treatment on the sliding velocity of live and demembranated spermatozoa. Sliding velocity is calculated as twice the product of beat frequency and mean bend angle, measured at the midpoint of the flagellar length (Brokaw, 1984*b*). Since attenuation of the bending waves represents a decease in bend angle of the bends propagating along the flagellum (see below), it might be expected that a measurement of sliding velocity

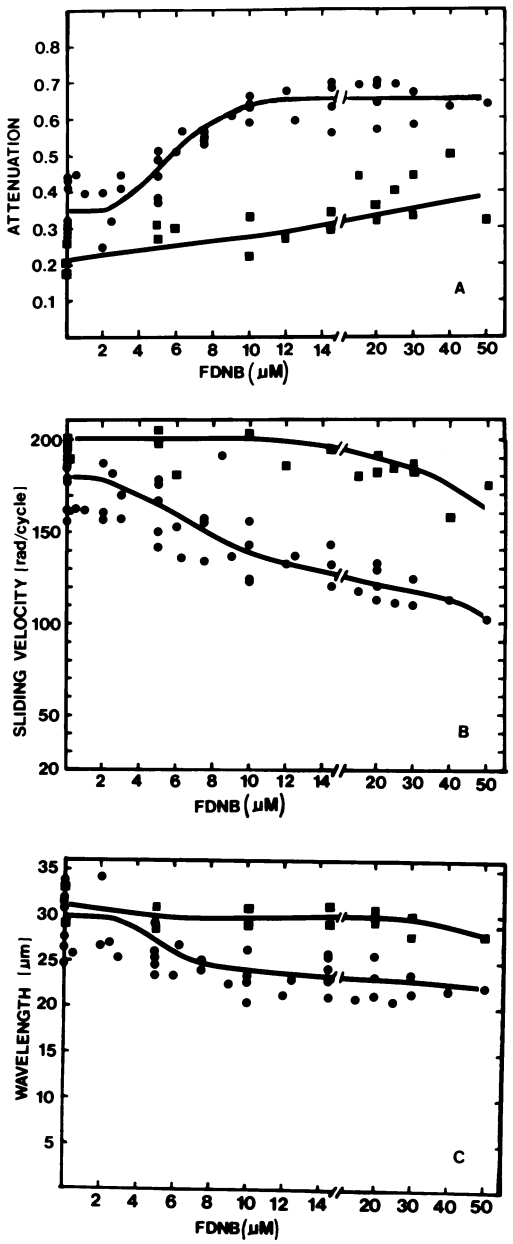

FIGURE 3 Plots of (*A*) bending wave attenuation, (*B*) mean sliding velocity, and (*C*) wavelength obtained from analysis of sample of spermatozoa after incubation with FDNB concentrations ranging from 0 to 50 μM. Each data point is from a sample of 20 spermatozoa. Data for live spermatozoa (●) and ATP-reactivated, demembranated spermatozoa (■) are shown in each plot. Standard deviation for the attenuation points ranged from 0.05 to 0.27, with a mean of 0.13. Standard deviations for the sliding velocity points ranged from 7 to 31, with a mean of 17 rad/s. Standard deviations for the wavelength points ranged from 0.8 to 3.9, with means of 1.5 μm for the live spermatozoa and 2.1 μm for the demembranated spermatozoa. Lines were drawn by eye as close as possible to the average data point at each FDNB concentration, while maintaining a smooth curve, to clarify our interpretation of the data.

at any point away from the basal region of the flagellum would show changes similar to the changes in attenuation. This, in fact, is observed in the data from live spermatozoa, which show the greatest decrease in sliding velocity in the region of 2–10 μM, paralleling the greatest increase in attenuation. However, the attenuation is a more sensitive measure of this effect of FDNB treatment. The data from demembranated, reactivated spermatozoa do not show any effect of FDNB treatment in the 0–10 μM range on sliding velocity. Both the live and demembranated spermatozoa show a gradual decrease in sliding velocity between 10 and 50 μM FDNB, which may be an indication of nonspecific FDNB effects on components other than CrK. The decrease in sliding velocity of live spermatozoa between 0 and 10 μM FDNB was largely the result of decreasing bend angle. Above 10 μM FDNB, the decrease in sliding velocity was largely caused by a decrease in beat frequency, with little additional decrease in bend angle (data not shown).

Inspection of photographs of severely attenuated waveforms, such as Fig. 1 *c*, gives the impression that the restriction of bending in the distal portion of the flagellum causes the active bending waves to be compressed into the basal portion of the flagellum, and therefore to have shorter wavelengths. This impression is supported by Fig. 3 *C*, which gives values of wavelength, calculated from the curvature values at the midpoint of the flagellar length, as a function of the concentration of FDNB treatment. With the live spermatozoa, there is a decrease in wavelength in the 2–10 μM concentration range, and little additional change at higher FDNB concentrations. There is little or no effect of FDNB treatment on the wavelength of the demembranated spermatozoa. FDNB treatment had no consistent effect on the asymmetry of the bending waves of live spermatozoa. With demembranated spermatozoa, FDNB-treated spermatozoa had slightly higher values of bending wave asymmetry (data now shown). Thus, in the 2–10 μM FDNB concentration range, the principal changes noted in the live sperm are related to attenuation, and these do not occur in demembranated cells.

Effects of FDNB Treatment on Flagellar CrK Activity

The results of measurements of CrK activity in the same sperm preparations used for the motility observations are shown in Fig. 4. Approximately 50% of the flagellar CrK activity is inhibited by treatment with 2 μM FDNB, the threshold concentration for observing effects on motility. Approximately 80% inhibition of CrK activity was observed after treatment with 6 μM FDNB, which gave a half-maximal increase in attenuation. Even at 50 μM FDNB, there is still a significant amount of residual CrK activity, and there is only a factor of two change in activity over the range from 10 to 50 μM FDNB. Purified CrK is not inhibited completely at these concentrations of FDNB (data not shown).

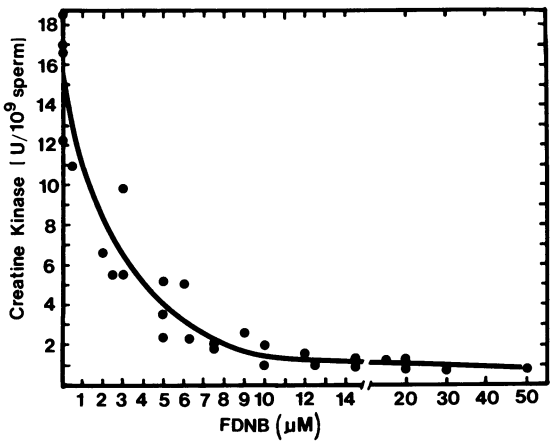

FIGURE 4 Measurements of CrK activity (reverse rate, Q_{3R}) of spermatozoa after incubation with FDNB concentrations ranging from 0 to 50 μM. 1 U = 1 μmol/min. Line drawn as in Fig. 3.

Interpretation of Bending Wave Attenuation

Ideally, we would like to use information on the attenuation of flagellar bending waves to deduce the ATP concentration profile along the sperm flagellum. Although it is possible for different regions of a flagellum, supplied with different concentrations of ATP, to beat independently with different frequencies (Brokaw and Gibbons, 1973), bending waves propagating along the full length of a flagellum must maintain a constant beat frequency. There are extensive data relating flagellar beat frequency to substrate ($MgATP^{-2}$) concentration. By analogy to muscle, where sliding velocity is determined by ATP concentration (Cooke and Bialeck, 1979), it is a reasonable expectation that the effect of ATP concentration on flagellar beat frequency reflects an effect on the velocity of sliding between flagellar microtubules. Experiments in which a demembranated flagellum was driven by an external oscillator at a fixed frequency should show a relationship between ATP concentration and bend angle; such experiments are technically feasible, but have not yet been reported. Nevertheless, we can asume that the local concentration of ATP at a point on a flagellum determines the velocity of microtubular sliding at that point, and that if the frequency is fixed, variations in sliding velocity must determine variations in the amplitude of the oscillatory sliding cycle and therefore the bend angle.

Variations in bend angle could be accommodated by variations in the curvature of the bends or in the length of the bends. The model that we have used for fitting these sea urchin sperm bending patterns (e.g., Fig. 2) assumes that the rates at which bends propagate along the flagellum are constant, so that the lengths of the propagating bends remain constant. Under these conditions, attenuation in curvature of the model (Fig. 2, *right*) will be seen if the bend angles of the flagellar bending waves are attenuated as they propagate along the flagellum. Inspection of the data for attenuated waves, Fig. 2, *B* and *C*, indicates that a decrease in curvature is more obvious than a decrease in wavelength, and suggests that our analysis procedure is reasonable.

If we interpret attenuation values in terms of sliding velocity, then a typical flagellum at 0–2 μM FDNB, where the sliding velocity at the midpoint of the length is 180 rad/s and the attenuation is 0.35, will have sliding velocities at the basal end and distal end of 218 and 142 rad/s, respectively. A typical flagellum at 10–15 μM FDNB, where the sliding velocity at the midpoint of the length is 130 rad/s and the attenuation is 0.65, will have sliding velocities at the basal end and distal end of 193 and 67 rad/s, respectively. In other words, the treatment with 10–15 μM FDNB reduces the sliding velocity at the distal end of the flagellum to about half its value in the absence of FDNB treatment. This result, and the observation of a threshold in FDNB effect, is consistent with the ATP concentration at the basal end of the flagellum being greater than 1 mM, well above the value of 0.11 mM which gives half-maximal beat frequency in the uninhibited flagella, and the ATP concentration at the distal end of the inhibited flagella being ~0.1 mM.

The situation is more complex in motile sperm, for several reasons. ADP is a competitive inhibitor of flagellar beat frequency, with a K_I equal to approximately twice the K_m for flagellar beat frequency (Okuno and Brokaw, 1979). If there is a substantial gradient of ATP along the flagellum to drive ~P transport, there must be a similar gradient of ADP in the opposite direction, and thus millimolar concentrations of ADP in the distal portion of the flagellum. This ADP will have a substantial inhibitory effect on the flagellar sliding velocity. Thus, we have used Eq. 2 to take into account effects of both ATP and ADP concentrations, as presented in the next section. Moreover, the sliding velocity at a particular locus on the flagellum is not entirely a result of the level of active sliding at that particular locus, but depends on the activity of other portions of this mechanically coupled system. In the most extreme case, active sliding in one region of a flagellum might initiate bending waves that could be passively propagated into other regions of the flagellum if the ATP concentration in those regions is sufficient to avoid rigor conditions. Whether the passive sliding resulting from this passively propagated bending would stimulate a level of ATPase greater than that expected from the local ATP and ADP concentrations is unknown. Therefore, use of the relationships between flagellar beat frequency and ATP and ADP concentrations to interpret the sliding velocity at the distal end of the flagellum with respect to [ATP] and [ADP] provides only an upper bound for the [ATP] at the distal end of the FDNB-treated flagella. An indication of the magnitude of this discrepancy can be obtained from the observation that in spermatozoa treated with 10–15 μM FDNB, respiration is inhibited by ~55% (Tombes and Shapiro, 1985). This is about twice the amount of inhibi-

tion that would be expected, since the inhibition of sliding velocity is ~50% at the distal end, and only 25–30% in the mid-region of the flagellum.

Calculation of ~P Diffusion along the Flagellum

Supply of ATP by diffusion along a flagellum or cilium has been analyzed previously by Brokaw (1966), Raff and Blum (1968), Nevo and Rikmenspoel (1970), Lin (1972), and Adam and Wei (1975). In the simplest case, where the ATPase reaction is considered to be zero order, there is a simple analytic solution for the steady-state ATP concentration as a function of length:

$$C = C_0 - sSQ/D + s^2Q/2D. \quad (6)$$

The concentration difference between the tip and the base is then $S^2Q/2D$. In this equation, C_0 is the concentration maintained at the base, s is position along the length, S is the total length, Q is the rate of ATPase, and D is the diffusion coefficient. Using a value of 150 $\mu m^2/s$ for the diffusion coefficient, based on values obtained for the diffusion of ATP in muscle fibers (Bowen and Martin, 1963, 1964; Kushmerick and Podolsky, 1969) and a value of 3.4 mM/s for the ATPase rate, then the required concentration difference for a flagellum 40 μm in length is 18 mM. A slightly higher concentration than 18 mM would therefore be required at the basal end of the flagellum to maintain a concentration at the tip that is high enough to justify the use of zero-order kinetics.

We have used numerical integration to obtain solutions for the diffusion equations for the more realistic situation where both adenylate kinase activity and CrK activity are involved in determining the concentrations of ATP, and where the inhibitory effect of ADP on flagellar ATPase activity and motility is considered. At the beginning of a computation, values for the equilibrium concentrations of the adenine nucleotide species at the base of the flagellum were calculated from the value of total adenine nucleotide concentration and the values of Cr and PCr for the base of the flagellum (Table I). These basal values were then used to initialize the concentrations of the diffusing species throughout the length of the flagellum. In effect, the computation was begun by turning on the ATPase activity at $t = 0$, and the differential equations were integrated forward in time until a steady-state equilibrium was obtained. Examples of some of the results are shown in Fig. 5. We have also used Eq. 2 to compute ATPase activity along the flagellum from ATP and ADP concentrations. The calculated ATPase rates can be used to calculate an ATPase attenuation value, which, like the curvature attenuation value, represents the fractional reduction in ATPase activity at the distal end of the flagellum, compared with that at the basal end, according to the following equation:

$$\text{ATPase attenuation} = 1 - \frac{\text{ATPase at distal end}}{\text{ATPase at basal end}}. \quad (7)$$

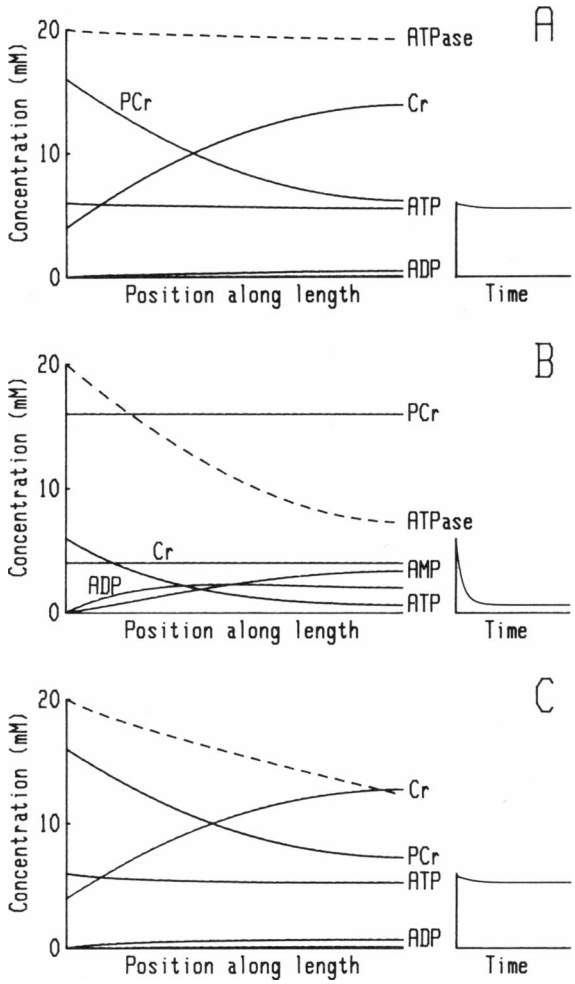

FIGURE 5 Examples of concentration profiles (*solid lines*) and ATPase activity profiles (*dashed lines;* no scale given) calculated for sperm flagella using the parameters given in Table I, with the following modifications: The CrK rates are: (*A*) Q_{3R} = 25.0 mM/s and Q_{3F} = 5.32 mM/s; (*B*) Both equal to 0; (*C*) Q_{3R} = 12.5 mM/s and Q_{3F} = 2.66 mM/s, and an intrinsic ATPase attenuation of 0.35 has been included. The resulting total ATPase attenuation is 0.39. Each computation was run for 30,000 time steps, to ensure that the steady-state equilibrium situation was reached; the small panels at the right show ATP concentration at the tip as a function of time.

Fig. 5 *A* illustrates the results of calculations of concentration profiles along the length of the flagellum, for a situation in which the CrK rate is high relative to the ATPase rate. Under these conditions, there are substantial gradients of Cr and PCr along the flagellum, very little change in ATP concentration along the length, and very little build-up of ADP in the distal portion of the flagellum. Consequently, the ATPase reaction rate is nearly uniform along the length of the flagellum; the ATPase attenuation value is only 0.04.

Fig. 5 *B* illustrates the results of calculations under similar conditions, except that the CrK rate has been reduced to zero. Under these conditions, there is a substantial ATP gradient along the flagellum, with the concentration falling from ~6 mM at the base to <1 mM at the tip.

Both ADP and AMP accumulate in the distal portion of the flagellum and their gradients both contribute to the return flux of adenine nucleotide to the mitochondrion. As a result of the accumulation of ADP in the distal portion of the flagellum, the ATPase rate at the distal end is only 36% of the ATPase rate at the basal end, giving an ATPase attenuation value of 0.64. The total ATPase rate for the flagellum is 60% of the amount in Fig. 5 *A*.

Computations with the parameters used for Fig. 5 *B* were carried out for flagella of various lengths. With the length increased to 50 μm, the ATPase attenuation value increases to 0.78. With the length decreased, the attenuation value becomes 0.47 for a length of 30 μm, 0.27 for a length of 20 μm, and 0.10 for a length of 10 μm. Thus, even for a flagellum with a length of only 20 μm, significant ATPase attenuation is observed in the absence of CrK activity, whereas it is not observed in a flagellum 40 μm in length with CrK activity.

Computations similar to Fig. 5, *A* and *B* were carried out for different CrK reaction rates. The resulting attenuation values were found to fall on a curve given by the following equation:

$$A = A_{min} + (A_{max} - A_{min})/\left(1 + \left(\frac{CrK}{K}\right)^n\right), \qquad (8)$$

where A represents ATPase attenuation, CrK represents the creatine kinase rate (Q_{3R}), and K and n are constants. Results obtained by fitting this equation to the data with a nonlinear least squares procedure are $K = 2.65$ mM/s, $n = 1.31$, minimum ATPase attenuation = 0.0, and maximum ATPase attenuation = 0.53. At high levels of CrK activity, this model does not give the relatively constant non-zero level of flagellar attenuation observed in untreated whole sperm. The 2 μM threshold effect suggests that the attenuation seen in the absence of FDNB does not represent a deficiency in energy transport along the flagellum.

A model matching the experimentally obtained flagellar attenuation results more closely can be obtained by adding an intrinsic ATPase attenuation such that the maximum ATPase rate used in this model, Q_{1F} in Eq. 2, decreases linearly along the length of the flagellum, so that there is a minimum ATPase attenuation of 0.35 even in the presence of high CrK rates. To give a mean value of Q_{1F} of 3.4 mM/s at the midpoint of the flagellum, Q_{1F} decreases from 4.12 mM/s at the base to 2.68 mM/s at the tip. Fig. 6 illustrates the relationship between ATPase attenuation and CrK rate obtained with this model and several different values of CrK. Fig. 5 *C* shows an example of metabolite profiles calculated by using a CrK value five times that leading to ATPase attenuation midway between the minimum (0.35) and maximum (0.73) values calculated by this model. This represents our best estimate of the conditions existing in normal spermatozoa, since we observed 80% inhibition of CrK activity with an FDNB concentration (6 μM), which gave a value of flagellar attenuation midway between the minimum and maximum

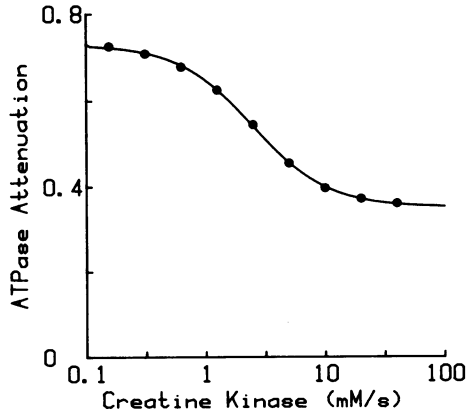

FIGURE 6 Results of computations of diffusion in a sperm flagellum with various rates of the CrK reaction. The results are shown as the calculated attenuation of the ATPase activity, for a model containing an intrinsic ATPase attenuation of 0.35, as in the example shown in Fig. 5 *C*. Parameters are given in Table I. The curve is obtained from Eq. 8, with the parameters given in the top row of Table II.

values observed experimentally as the FDNB concentration was varied.

Table II gives the parameters obtained by fitting Eq. 8 to the results of computations similar to Fig. 6, with the parameters of the model varied to test the sensitivity of the model. The major parameters affecting the results are the ATPase rate, the total adenine nucleotide concentration, and the diffusion coefficients; these of course are the parameters that would remain in the simplest models that neglect ADP inhibition and adenylate kinase. Variations in total adenine nucleotide concentration in individual spermatozoa would appear to be the most likely explanation for the variation in values of flagellar waveform attenuation measured with individual spermatozoa. The model is also relatively sensitive to the substrate affinities for the CrK reverse reaction, but the exact values of the other parameters have only minor effects on the results.

DISCUSSION

Specificity of CrK Inhibition by FDNB

Our interpretation of the effects of FDNB on the bending waves of sea urchin sperm flagella depends upon the assumption that, under the conditions of our experiments, inhibition of CrK is the only significant effect of FDNB. This assumption rests on evidence presented earlier (Tombes and Shapiro, 1985) comparing the in vitro inhibition of CrK, adenylate kinase, and dynein ATPase by incubation of spermatozoa with FDNB. These measurements showed that for FDNB concentrations up to 15 μM, only the CrK activity was significantly inhibited. Additional evidence was provided by comparing the motility of live and demembranated spermatozoa, and showing that only with live spermatozoa, where CrK would be important in providing ATP to the flagellum, was there an inhibition of flagellar motility after treatment with low concentra-

TABLE II
PARAMETERS SUMMARIZING THE RELATIONSHIP BETWEEN ATPase ATTENUATION AND CrK RATES

Conditions	A_{min}	A_{max}	K	n
			mM/s	
Standard (Table I)	0.35	0.73	2.52	1.38
Total adenine nucleotide concentration reduced to 3 mM	0.35	0.87	2.41	1.46
Reduced D for Cr and PCr; $D_P = D_A = 150\ \mu m^2/s$	0.40	0.74	2.25	1.26
Both D reduced by ½; $D_P = 130$, $D_A = 75\ \mu m^2/s$	0.47	0.87	1.85	1.44
ATPase and adenylate kinase rates reduced by ½; Q_1 and $Q_2 = 1.7$ mM/s	0.35	0.59	1.43	1.50
ATPase affinity for ATP and ADP increased by 2; $K1 = 0.055$ mM, $K_1 = 0.11$ mM	0.35	0.73	2.53	1.36
ATPase affinity for ADP reduced by ½; $K_1 = 0.44$ mM	0.35	0.72	1.94	1.43
Adenylate kinase activity reduced by ¼; $Q_2 = 0.85$ mM/s	0.35	0.78	2.32	1.41
Adenylate kinase activity reduced by 1/100; $Q_2 = 0.034$	0.35	0.87	2.29	1.50
CrK forward rate increased by 2; $Q_{3F} = Q_{3R}/2.35$	0.36	0.73	2.48	1.37
CrK affinity for PCr reduced by ½; $K_P = 0.012$ M	0.36	0.74	3.48	1.23
CrK affinity for ADP reduced by ½; $K_D = 0.00024$ M	0.36	0.74	2.86	1.23
CrK affinity for PCr and ADP reduced by ½; $K_P = 0.012$ M, $K_D = 0.00024$ M	0.36	0.74	4.05	1.12

Obtained by computations of diffusion along a flagellum and fitting the results with Eq. 8 in the text. Parameters varied included diffusion coefficients (D), and other enzymatic parameters (see Table I).

tions of FDNB (Tombes and Shapiro, 1985). We have used more detailed analysis of flagellar bending patterns to extend these comparisons of FDNB effects on live and demembranated spermatozoa. Our new data confirm that the effects on live spermatozoa specifically associated with an inhibition of CrK activity are not detectable with demembranated spermatozoa that are uniformly bathed in solutions containing adequate ATP concentrations. Effects that are seen with demembranated spermatozoa after incubation with FDNB are only found above 15 μM FDNB and differ qualitatively from the effects seen with live spermatozoa after treatment with FDNB in the 0–15 μM concentration range. We therefore feel confident in interpreting the changes in flagellar bending patterns that are seen in live spermatozoa after treatment with FDNB concentrations of up to 15 μM as the result of a specific inhibition of flagellar CrK activity.

Characterization of Attenuated Flagellar Bending Waves Resulting from CrK Inhibition

The bending waves of these sea urchin sperm flagella can be modeled more closely by assuming that the curvatures of the propagating bends (and consequently, the bend angles and the sliding velocity) decrease linearly along the length of the flagellum. This decrease can be described by the parameter that we have called attenuation. Significant attenuation was measured in all samples of spermatozoa not exposed to FDNB. Since this attenuation did not increase with treatments up to 2 μM FDNB, which inhibited up to 50% of the CrK activity, we suggest that the attenuation seen in normal spermatozoa is not indicative of deficient energy transport along the flagellum. Sea urchin spermatozoa consistently generate bends with higher curvature near the basal end of the flagellum, which then lengthen and decrease in curvature as they begin to propagate along the flagellum (Brokaw, 1965). Even though this does not give a linear decrease in curvature along the flagellum, it would be expected to influence our curve-fitting process and to cause the analysis of normal bending patterns to produce non-zero attenuation values.

After incubation with FDNB, the average value of attenuation in the sperm samples increases significantly. We interpret this as a decrease in the velocity of sliding between flagellar microtubules in the distal regions of the flagellum. This is supported by measurements indicating that there is a decrease in the average sliding velocity (measured at the midpoint of the flagellar length), which varies with FDNB concentration in the same way as the attenuation. The sliding velocity in the distal end of the flagellum can result from both locally generated active sliding and passive sliding resulting from activity in more proximal regions of the flagellum. Therefore, we cannot obtain the direct measure of the attenuation of active sliding along the flagellum that would be desirable for comparison with ATP and ADP concentrations. Comparison with the overall inhibition of sperm respiration by FDNB treatment suggests that the attenuation of active sliding should be no more than twice as great as the attenuation given by our measurements.

In addition to the attenuation of sliding velocity that can be related to the supply of ATP along the flagellum, our analysis also reveals that the FDNB-inhibited spermatozoa generate bending patterns with shorter wavelengths. This effect is not graded along the flagellum, and a decrease in wavelength is not seen when demembranated spermatozoa are exposed to ADP or to reduced ATP concentrations (Brokaw, 1975; Okuno and Brokaw, 1979). The wavelength effect must be a secondary effect resulting from or associated with the attenuation of sliding velocity in the distal portion of the flagellum. Its interpretation will require detailed modeling of mechanisms for flagellar wave generation (e.g., Brokaw, 1972, 1985) and is beyond the scope of the present paper.

Quantitative Analysis of Energy Transport in Sperm Flagella

Our analysis of energy transport by diffusion along a sperm flagellum is the first complete analysis that consid-

ers the participation of PCr and CrK, in addition to ATP, ADP, and the ATPase and adenylate kinase reactions, and also considers the inhibitory effect of ADP accumulation in the flagellum. Recently, a CrK-facilitated diffusion model was tested for cylindrical muscle fibers of varying diameters (Meyer et al., 1984). Our analysis reveals the importance of PCr transport in preventing the accumulation of inhibitory levels of ADP in the distal portion of the flagellum, in addition to maintaining adequate levels of ATP. The adenylate kinase can at best reduce the ADP accumulation by a factor of two. Inclusion of the inhibitory effect of ADP in the analysis shows that ~P transport by PCr is important even in flagella as short as 20 μm, whereas a simple analysis of ATP diffusion, using Eq. 6, would suggest that ATP diffusion alone would be adequate.

Fig. 5 *C* summarizes our model for energy transport in a sea urchin sperm flagellum under conditions of normal motile activity. It shows substantial gradients of PCr and Cr, and PCr diffusion must clearly be the major route for ~P transport along the flagellum. Irrespective of whether ~P is carried by diffusion of PCr or ATP, there must be an equivalent reverse transport of inorganic phosphate (P_i) back to the basal end of the flagellum, and a sufficient P_i concentration gradient to drive this transport. We have not calculated this gradient, since it is clear that given the high P_i concentrations that have been observed in these spermatozoa (Christen et al., 1983*b*) and the higher diffusion coefficient for this small species, diffusion of P_i will not be a limiting factor.

This model was developed to better understand the transport of energy along the sperm flagellum and is not intended to be a complete model of sperm energetics. It effectively assumes an infinite source of ATP that maintains the initial ATP concentration at the base of the flagellum. It does not consider the increased ADP concentration and decreased ATP concentration that will be required at the sperm mitochondrion to stimulate ATP production in accordance with observations that respiratory rates in actively swimming spermatozoa are maximal and cannot be increased by mitochondrial uncoupling agents (Christen et al., 1982; Tombes and Shapiro, 1985). Similarly, it fails to incorporate the observation that mean sperm ATP concentration falls to 1–2 mM upon activation of motility and respiration (Christen et al., 1983*a*; Mita and Yasumasu, 1983). An expanded model incorporating these considerations would be of great interest, but would require information and assumptions about the regulation of sperm metabolism that are beyond the scope of the present work.

Our analysis also allows us to obtain a quantitative estimate of the level of CrK activity in a flagellum that would be consistent with the experimentally observed effect of CrK inhibition on waveform attenuation. A half-maximal effect on waveform attenuation was observed after treatment with 6 μM FDNB (Fig. 3 *A*), where the CrK activity was inhibited by 80%. The diffusion computations showed a half-maximal ATPase attenuation with CrK activity (Q_{3R}) = 2.5 mM/s (Fig. 6). By this approach, we can estimate 12.5 mM/s for the normal CrK reverse rate in the sperm flagella. This estimate is uncertain within a factor of two because of the inability to discriminate between active and passive sliding in the distal portion of the flagellum, as discussed previously.

Biochemical measurements of the flagellar CrK activity of these spermatozoa (Tombes and Shapiro, 1985) gave 3.8 μmol/min per 10^9 sperm tails, which converts to a rate of 51 mM/s. However, this value needs to be adjusted for the difference between the conditions used for the assay and the conditions within the sperm flagellum. Adjustment for the lower pH (pH 7.5) within the spermatozoon (Christen et al., 1982) requires a 50% reduction in CrK activity (Tombes, R. M., unpublished measurements). Adjustment for the 20 mM P_i concentration found within motile spermatozoa (Christen et al., 1983*b*), requires a 30% reduction in CrK activity. Together, these reduce the measured value to ~18 mM/s, which is within a factor of two of our estimate from the observations on motility. We believe that this agreement is good enough to provide further support for the conclusion that CrK activity and PCr diffusion are essential for the generation of normal bending waves by sea urchin sperm flagella.

We are grateful to Sandy Nagayama and Larry Jones for technical assistance and to Mary Patella for typing assistance.

This work was supported by National Institutes of Health grants GM-23910 to B. M. Shapiro, HDO-7183-06 to R. M. Tombes, and GM-18711 to C. J. Brokaw.

Received for publication 7 July 1986 and in final form 12 March 1987.

REFERENCES

Adam, D. E., and J. Wei. 1975. Mass transport of ATP within the motile sperm. *J. Theor. Biol.* 49:125–145.

Baccetti, B., and B. A. Afzelius. 1976. The biology of the sperm cell. *Monogr. Dev. Biol.* 10:65–80.

Bowen, W. J., and H. L. Martin. 1963. A study of diffusion of ATP through glycerol-treated muscle. *Arch. Biochem. Biophys.* 102:286–292.

Bowen, W. J., and H. L. Martin. 1964. The diffusion of ATP through aqueous solutions. *Arch. Biochem. Biophys.* 107:30–36.

Brokaw, C. J. 1965. Non-sinusoidal bending waves of sperm flagella. *J. Exp. Biol.* 43:155–169.

Brokaw, C. J. 1966. Mechanics and energetics of cilia. *Am. Rev. Respir. Dis.* 93:32–40.

Brokaw, C. J. 1967. Adenosine triphosphate usage by flagella. *Science (Wash. DC).* 156:76–78.

Brokaw, C. J. 1972. Computer simulation of flagellar movement. I. Demonstration of stable bend propagation and bend initiation by the sliding filament model. *Biophys. J.* 12:564–586.

Brokaw, C. J. 1975. Effects of viscosity and ATP concentration on the movement of reactivated sea urchin sperm flagella. *J. Exp. Biol.* 62:701–719.

Brokaw, C. J. 1983. The constant curvature model for flagellar bending patterns. *J. Submicrosc. Cytol.* 15:5–8.

Brokaw, C. J. 1984*a*. Cyclic AMP-dependent activation of sea urchin and tunicate sperm motility. *Ann. NY Acad. Sci.* 438:132–141.

Brokaw, C. J. 1984*b*. Automated methods for estimation of sperm flagellar bending patterns. *Cell Motil.* 4:417–430.

Brokaw, C. J. 1985. Computer simulation of flagellar movement. VI. Simple curvature-controlled models are incompletely specified. *Biophys. J.* 48:633–642.

Brokaw, C. J. 1986. Sperm motility. Echinoderm gametes and embryos. *Methods Cell Biol.* 27:41–56.

Brokaw, C. J., and I. R. Gibbons. 1973. Localized activation of bending in proximal, medial, and distal regions of sea urchin sperm flagella. *J. Cell Sci.* 14:1–10.

Brokaw, C. J., and I. R. Gibbons. Mechanisms of movement in flagella and cilia. *In* Swimming and Flying in Nature. T. T. Wu, C. J. Brokaw, and C. Brennan, editors. Plenum Publishing Corp., New York. 89–126.

Christen, R., R. W. Schackmann, and B. M. Shapiro. 1982. Elevation of the intracellular pH activates respiration and motility of sperm of the sea urchin, *Strongylocentrotus purpuratus*. *J. Biol. Chem.* 256:14881–14890.

Christen, R., R. W. Schackmann, and B. M. Shapiro. 1983*a*. Metabolism of sea urchin sperm: interrelationships between intracellular pH, ATPase activity and mitochondrial respiration. *J. Biol. Chem.* 258(9):5392–5399.

Christen, R., R. W. Schackmann, F. W. Dahlquist, and B. M. Shapiro. 1983*b*. ^{31}P-NMR analysis of sea urchin sperm activation: reversible formation of high energy phosphate compounds by changes in intracellular pH. *Exp. Cell Res.* 149:289–294.

Cooke, R., and W. Bialek. 1979. Contraction of glycerinated muscle fibers as a function of the ATP concentration. *Biophys. J.* 28:241–258.

Gibbons, B. H., and I. R. Gibbons. 1972. Flagellar movement and adenosine triphosphatase activity in sea urchin sperm extracted with Triton X-100. *J. Cell Biol.* 54:75–97.

Gibbons, B. H., W. Y. Tang, and I. R. Gibbons. 1985. Organic anions stabilize the reactivated motility of sperm flagella and the latency of dynein 1 ATPase activity. *J. Cell Biol.* 101:1281–1287.

Gibbons, I. R. 1981. Cilia and flagella of eukaryotes. *J. Cell Biol.* 91(3,Pt.2):107s–124s.

Hansbrough, J. R., G. S. Kopf, and D. L. Garbers. 1980. The stimulation of sperm metabolism by a factor associated with eggs and by 8-bromo-guanosine 3',5'-monophosphate. *Biochem. Biophys. Acta.* 630:82–91.

Kushmerick, M. J., and R. J. Podolsky. 1969. Ionic mobility in muscle cells. *Science (Wash. DC).* 166:1297–1298.

Lin, S. W. 1972. Transient analysis of dual enzyme reaction in cilia. *Biophysik.* 8:264–270.

Meyer, R. K., H. L. Sweeney, and M. J. Kushmerick. 1984. A simple analysis of the "phosphocreatine shuttle." *Am. J. Physiol.* 246:C365–C377.

Mita, M., and I. Yasumasu. 1983. Metabolism of lipid and carbohydrate in sea urchin spermatozoa. *Gamete Res.* 7:133–144.

Nevo, A. C., and R. Rikmenspoel. 1970. Diffusion of ATP in sperm flagella. *J. Theor. Biol.* 26:11–18.

Noda, L. 1973. Adenylate kinase. *In* The Enzymes. Vol. VIIIA. P. D. Boyer, editor. Academic Press, Inc., New York. 279–305.

Okuno, M., and D. J. Brokaw. 1979. Inhibition of movement of Triton-demembranated sea urchin sperm flagella by Mg^{2+}, ATP^{4-}, ADP and P_i. *J. Cell Sci.* 38:105–123.

Penningroth, S. M., A. Cheung, K. Olehnik, and R. Koslosky. 1982. Mechanochemical coupling in the relaxation of rigor-wave sea urchin sperm flagella. *J. Cell Biol.* 92:733–741.

Raff, E. C., and J. J. Blum. 1968. A possible role for adenylate kinase in cilia: concentration profiles in a geometrically constrained dual enzyme system. *J. Theor. Biol.* 18:53–71.

Rothschild, Lord, and K. W. Cleland. 1952. The physiology of sea urchin spermatozoa. The nature and location of the endogenous substrate. *J. Exp. Biol.* 29:66–71.

Schackmann, R. W., R. Christen, and B. M. Shapiro. 1984. Measurement of plasma membrane and mitochondrial potentials in sea urchin sperm: changes upon activation and induction of the acrosome reaction. *J. Biol. Chem.* 259:13914–13922.

Tombes, R. M., and B. M. Shapiro. 1985. Metabolite chanelling: a phosphocreatine shuttle to mediate high energy phosphate transport between sperm mitochondrion and tail. *Cell.* 41:325–334.

Warner, F. D., and D. R. Mitchell. 1980. Dynein: the mechanochemical coupling adenosine triphosphatase of microtubule-based sliding filament mechanisms. *Int. Rev. Cytol.* 66:1–43.